npj | Climate and Atmospheric Science

Supplementary Figures

Causes of 2022 Pakistan flooding and its linkage with China and Europe heatwaves

Chi-Cherng Hong[1], An-Yi Huang[1], Huang-Hsiung Hsu[2*], Wan-Ling Tseng[2,3], Mong-Ming Lu[4], Chih-Chun Chang[1]

[1]Department of Earth and Life Science, University of Taipei, Taipei, Taiwan.

[2]Anthropogentic Climate Change Center, Research Center for Environmental Changes, Academia Sinica, Taipei, Taiwan.

[3]International Degree Program in Climate Change and Sustainable Development, National Taiwan University, Taipei, Taiwan.

[4]Department of Atmospheric Sciences, National Taiwan University, Taipei, Taiwan.

*Corresponding author:

Dr. Huang-Hsiung Hsu, Research Center for Environmental Change, Academia Sinica, 128 Academia Road, Section 2, Nankang, Taipei, 115, Taiwan

E-Mail: hhhsu@gate.sinica.edu.tw

Supplementary Table 1. A comparison of large-scale atmospheric and oceanic conditions between 1998, 1999, 2010, 2020, and 2022. The magnitude terminologies of weak, moderate, and strong are based on their normalized index values (weak: >=0.5 and <1 or <=-0.5 and >-1; moderate: >=1 and <1.5 or <=-1 and >-1.5; strong: >=1.5 or <=-1.5). The PKT rainfall, tropical Pacific SST (Niño3.4), WNPSH, and Northern Indian subcontinent easterly are defined as anomalous precipitation averaged over 22°–32°N, 63°–73°E, SST averaged over 5°S–5°N, 170°–120°W, 850-hPa streamfunction averaged over 15°–25°N, 115°–140°E, and 850-hPa horizontal wind averaged over 15°–25°N, 70°–90°E.

	1998	**1999**	**2010**	**2020**	**2022**
PKT rainfall	Weak	Weak	Strong (3$^{\text{rd}}$)	Strong (2$^{\text{nd}}$)	Very strong (1$^{\text{st}}$)
Tropical Pacific SST	Moderate La Niña	Strong La Niña	Strong La Niña	Neutral	Moderate La Niña
WNPSH	Strong	Weak	Strong, extended northward	Strong, extended westward	Strong, extended westward
Northward propagation of convection (OLR)	Not evident	Not evident	Yes	Yes	Yes
Northern Indian subcontinent easterly	Weak	Not evident	Strong	Moderate	Strong
Mid-latitude blocking (location)	Siberian	Not evident	Northern European	Not evident	North Eastern European
Tropical-extratropical interaction	Not evident	Not evident	Yes	Weak	Yes

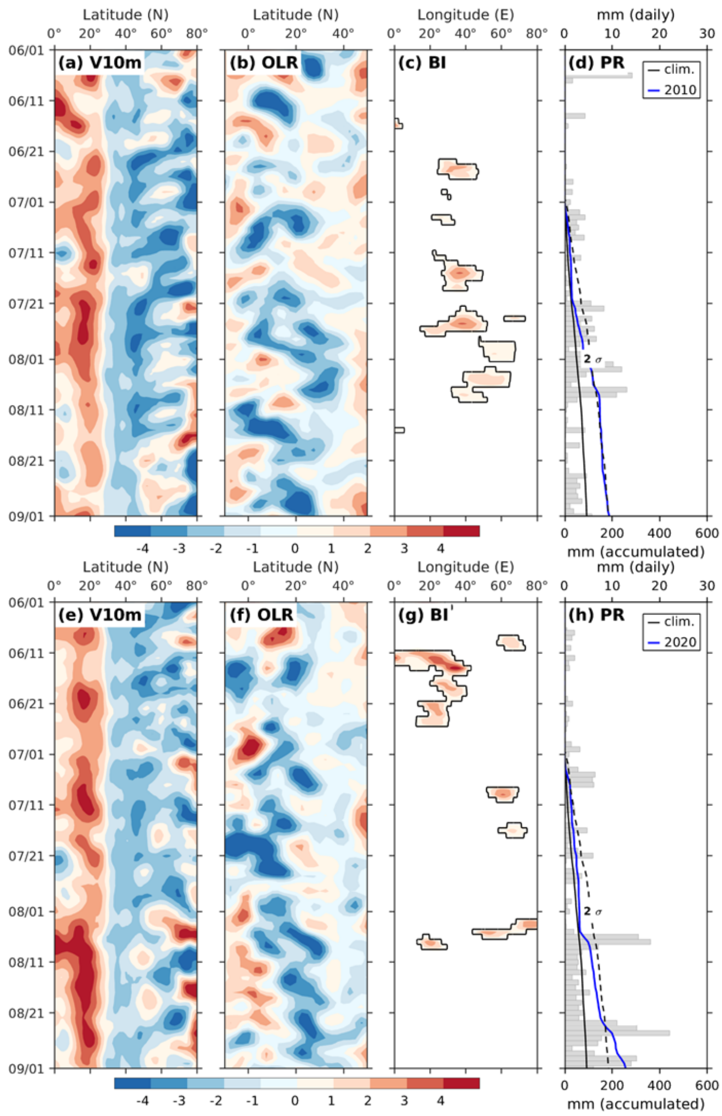

Supplementary Figure 1. Time evolution of 2010 Pakistan extreme rainfall and associated large-scale conditions (from June 1st to September 1st). (a) Hovmöller diagram of 3-day averaged 10-m meridional wind (V10m, shading; unit: $m{\cdot}s^{-1}$) averaged over 60°–75°E. (b) Same as (a), but for anomalous outgoing longwave radiation (OLR, shading; unit: 10^1 $W{\cdot}m^{-2}$). White arrows indicate the northward propagation of convection. (c) Shading represents the 500-hPa geopotential height gradient south of middle-high latitude (blocking index, BI; unit: m/degree latitude; only values larger than 0 are plotted) averaged over 5 grid points (details are documented in the methods section). Black contour lines (0 isoline) mark the regions of blocking. (d) Bars and lines represent daily and accumulated PKT rainfall (PR; unit: $mm{\cdot}day^{-1}$), respectively. The colored bars indicate three waves of extreme rainfall periods (surge 1 in green: 7/1–7/18, surge 2 in yellow: 7/23–7/30, and surge 3 in blue: 8/4–8/30). The numbers near colored bars are the percentage of the accumulated rainfall in each period against total period (7/1–8/31). (e–h) Same as (a–d), but for 2020.

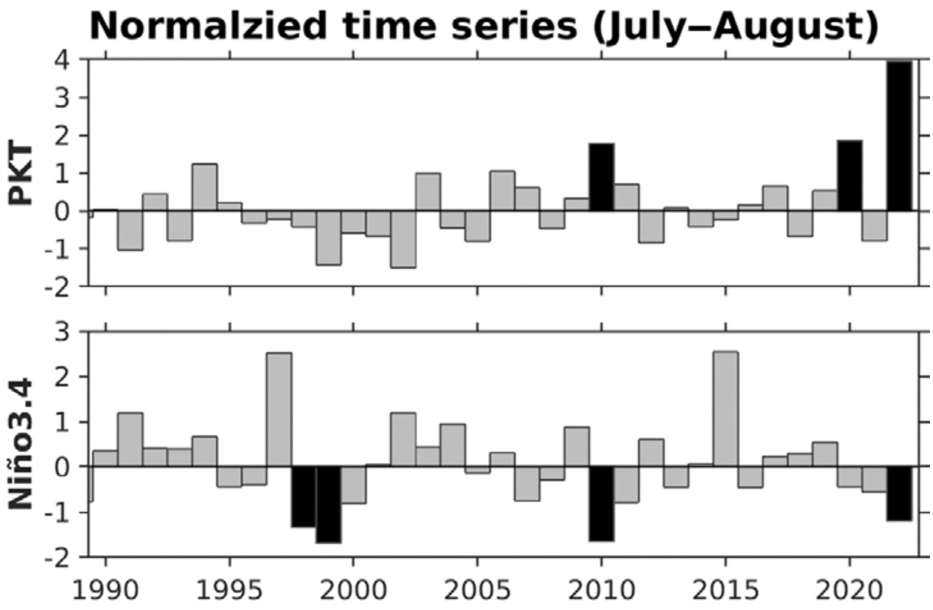

Supplementary Figure 2. Normalized time series of PKT index and Niño3.4 indices. (upper panel) PKT index is defined as July–August averaged precipitation (unit: mm·day^{-1}) anomaly over 22°–32°N, 63°–73°E. Values of years (2010, 2020, and 2022) marked as black bars are larger than 1.5 standard deviation. (lower panel) Same as (upper panel), but for Niño3.4 index, which is defined as sea surface temperature (unit: °C) anomaly over 170°–120°W, 5°S–5°N. Values of years (1998, 1999, 2020, and 2022) marked as black bars are less than -1 standard deviation.

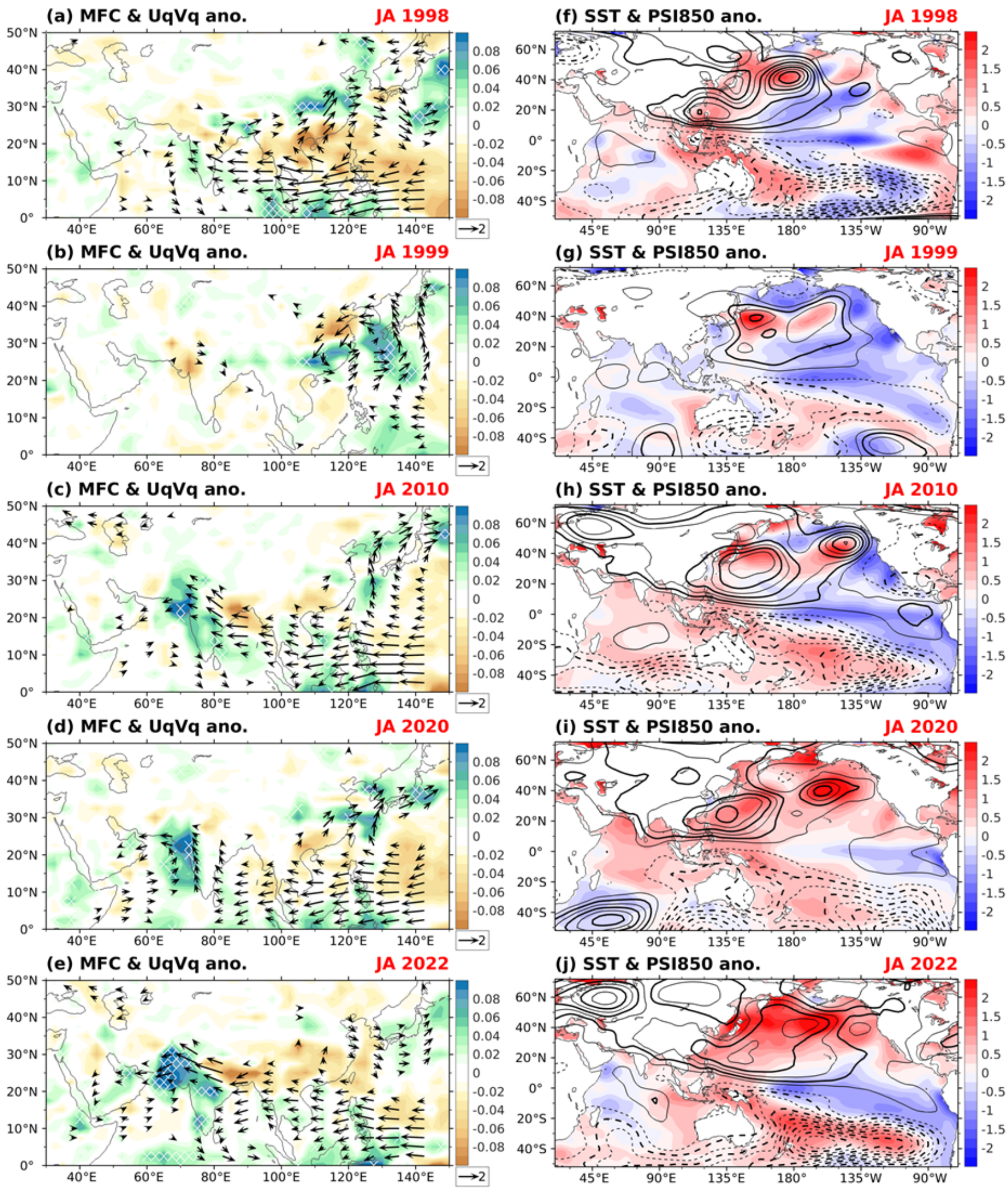

Supplementary Figure 3. Comparison of July–August (JA) averaged anomalous background conditions in 1998, 1999, 2010, 2020, and 2022. (a) Vertically integrated (surface–300-hPa) moisture flux convergence (MFC, shading; unit: $g \cdot m^{-2} \cdot s^{-1}$) and moisture flux (UqVq, vectors; unit: 10^5 $g \cdot m^{-1} \cdot s^{-1}$; minimum vector: 0.5) in 1998. Note that the values of MFC had been multiplied by "-1" (i.e., positive and negative values represent convergence and divergence, respectively). (b–e) Same as (a), but for 1999, 2010, 2020, and 2022, respectively. (f) Sea surface temperature (SST, shading; unit: °C) and 850-hPa streamfunction (PSI850, contour; unit 10^6 $m^2 \cdot s^{-1}$; interval: 1) in 1998. (g–j) Same as (f), but for 1999, 2010, 2020, and 2022, respectively. Shadings with white crosses in (a–e) indicate that the signals (MFC) of each grid exceed the 99th percentile during 1979–2022.

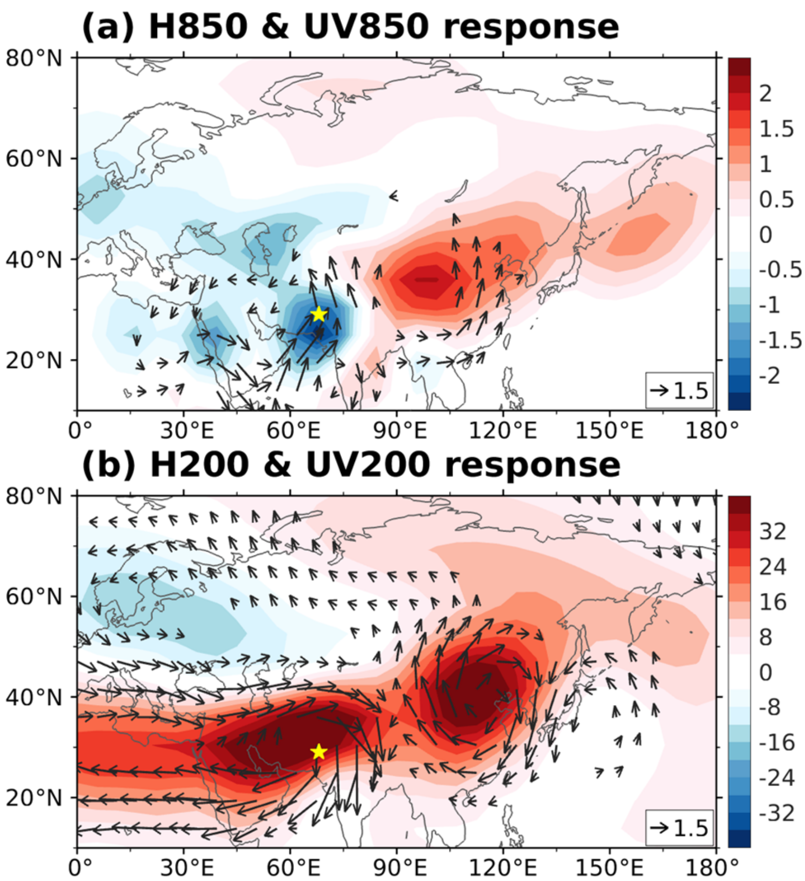

Supplementary Figure 4. Atmospheric response to an idealized heating over Pakistan. (a) Lower-level response at the 30th day (Linear Baroclinic Model[40]). Shading and vectors represent 850-hPa geopotential height (H850; unit: m) and horizontal winds (UV850; m·s^{-1}; minimum vector: 0.6) anomalies. The yellow star indicates the idealized heating center. (b) Same as (a), but for 200-hPa geopotential height (H200) and horizontal winds (UV200).

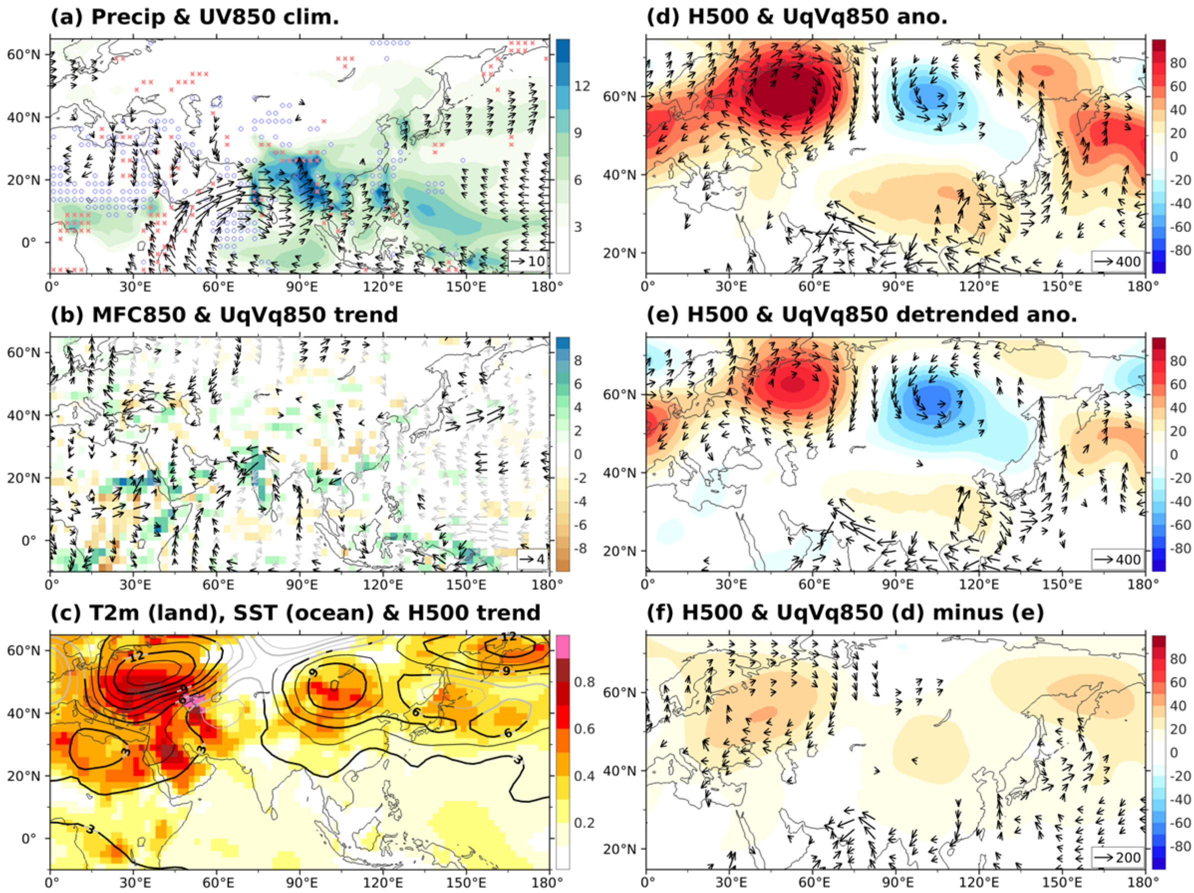

Supplementary Figure 5. Contribution of long-term linear trends. (a) July–August monthly averaged climatological state (1981–2010) of precipitation (PR, shading; unit: mm·day^{-1}) and 850-hPa horizontal winds (UV850, vectors; unit: m·s^{-1}; minimum vector: 3.5) in boreal summer. The precipitation marked by blue circles (red crosses) indicate the yearly precipitation with significantly (exceeding 90% confidence level based on the Student's *t*-test) upward (downward) trend during 1979–2021. (b) Linear trend (regression coefficients) of July–August monthly averaged 850-hPa moisture flux convergence (MFC850, shading; unit: 10^{-6} g·kg^{-1}·s^{-1} per decade) and moisture flux (UqVq850, vectors; unit: m·s^{-1} g·kg^{-1} per decade; minimum vector: 0.1). Note that the values of MFC had been multiplied by "-1" (i.e., positive and negative values represent convergence and divergence, respectively). Shadings and black vectors depict the regression coefficients exceed 90% confidence level based on the Student's *t*-test. (c) Same as (b), but for 2-m temperature (T2m, shading over land; unit: °C per decade), sea surface temperature (SST, shading over ocean; unit: °C per decade), and 500-hPa geopotential height (H500, contour; unit: m per decade; interval: 1.5). Shadings and black contour lines depict the regression coefficients exceed 90% confidence level based on the Student's *t*-test. (d) 2022 July 1st to August 1st daily averaged anomalous 500-hPa geopotential height (H500, shading; unit: m) and 850-hPa moisture flux (UqVq850, vectors; unit: m·s^{-1} g·kg^{-}

^{1}; minimum vector: 100). (e) Same as (d), but for detrended anomalies (after removing linear trend during 1979–2022). (f) Same as (d), but for the trend contribution by simply subtracting (e) from (d) (minimum vector: 50).

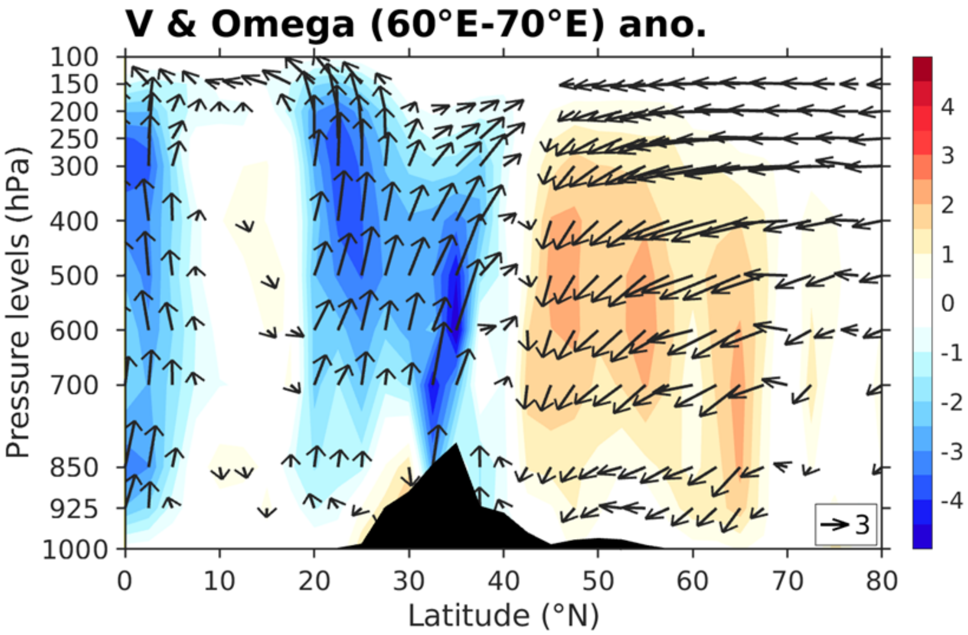

Supplementary Figure 6. Vertical-meridional circulation anomaly in 2022. July–August averaged anomalous vertical velocity (Omega, shading; unit: 10^2 Pa·s^{-1}) and meridional wind (V; unit: m·s^{-1}) averaged over 60°–70°E. Vectors represent V and negative Omega (minimum vector: 1.2). Black shading denotes mountain area (surface pressure; unit: hPa).

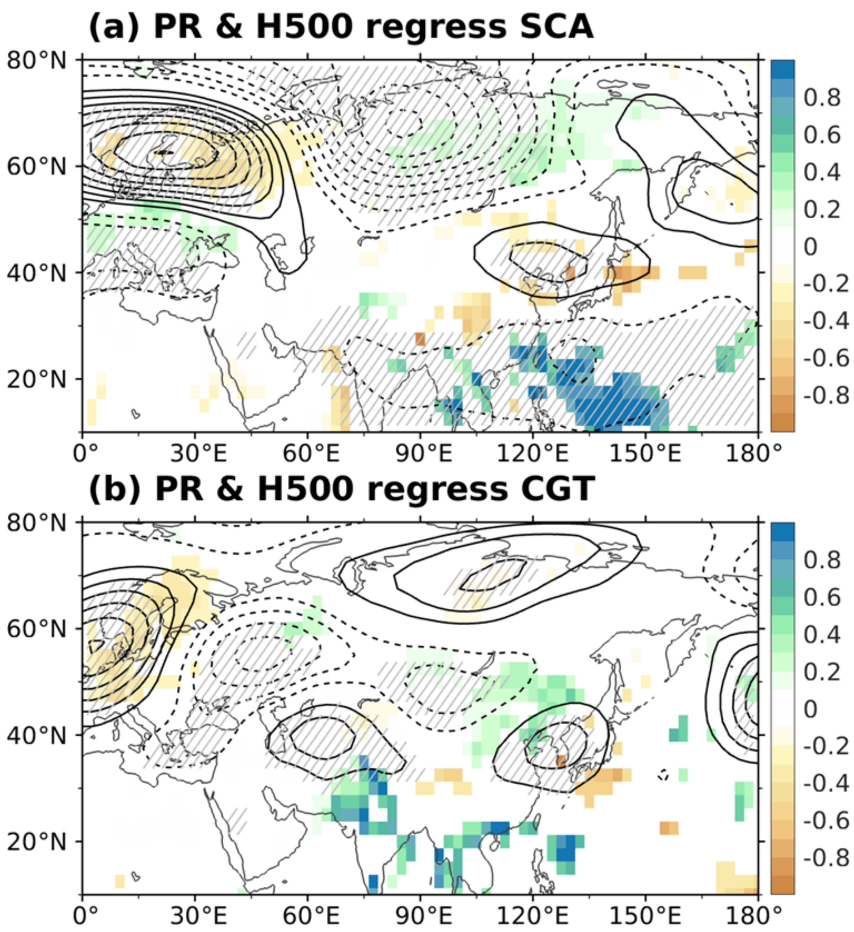

Supplementary Figure 7. Scandinavia (SCA) and circumglobal teleconnection (CGT) patterns. (a) Regression coefficients of July–August averaged precipitation (shading) and 500-hPa geopotential height (contour; interval: 3) on normalized SCA index (from https://www.cpc.ncep.noaa.gov/data/teledoc/telecontents.shtml) during 1979–2021. Shadings and hatched regions indicate the regression coefficients exceed 90% confidence level based on Student's *t*-test. (b) Same as (a), but on normalized CGT index (defined as 200-hPa geopotential height anomaly averaged over 35°–40°N, 60°–70°E according to Ding and Wang's paper[30]).